Journal of Nano- and Electronic Physics
Vol. **14** No 5, 05012(8pp) (2022)

Журнал нано- та електронної фізики
Том **14** № 5, 05012(8cc) (2022)

Study of Mono- and Polycrystalline Silicon Solar Cells with Various Shapes for Photovoltaic Devices in 3D Format: Experiment and Simulation

J. Gulomov*, R. Aliev, N. Mirzaalimov, B. Rashidov, J. Alieva

Andijan State University, 129, Universitet St., 170100 Andijan, Uzbekistan

(Received 03 August 2022; revised manuscript received 22 October 2022; published online 28 October 2022)

When the temperature increases, the efficiency of solar cells decreases, so the construction and design of photovoltaic devices with a cooling system from solar cells instead of solar panels is one of the most important tasks today. Therefore, in this scientific work, various forms of photoelectric devices in 3D format that can cool themselves by rotating around their own axis were studied. In these devices, mainly triangular and rectangular solar cells are used, so the effect of the cross-sectional shape on the photoelectric parameters of monocrystalline and polycrystalline silicon-based solar cells has been studied experimentally and with simulation. The results showed that polycrystalline silicon-based solar cells can be cut rectangular and used in the manufacture of prism-shaped photovoltaic devices, as well as monocrystalline silicon-based solar cells can be used in triangular cutting and in the manufacture of pyramid-shaped photovoltaic devices. Based on these results, a hexagonal prism-shaped photoelectric device made of a rectangular polycrystalline silicon-based solar cell was studied experimentally. The surface temperature of the device was 50 °C without rotation and the open circuit voltage was 13.12 V. In the range of 0-6 rad/s of rotation speed, the open circuit voltage of the device increased sharply by 0.36 V and the surface temperature decreased by 9.4 °C.

Keywords: Monocrystal, Polycrystal, Silicon, Solar cell, Photovoltaic device, Simulation, Shape.

DOI: 10.21272/jnep.14(5).05012 PACS numbers: 85.60.Bt, 78.20.Bh, 84.60.Jt

1. INTRODUCTION

Today, the focus is on the use of renewable energy sources to meet the demand for electricity [1] because most of the non-renewable energy sources on earth are declining and their use has a negative impact on the environment. There are three main sources of renewable energy sources: water, solar and wind [2].

Solar cells are mainly used to convert light energy from the sun into electricity. There are many types of solar cells, but in the industry, silicon-based solar cells are mainly produced [3]. The maximum efficiency of silicon-based solar cells is 26 % in experiment [4] and 29 % in theory [5].

A lot of complex research is being done to increase the efficiency of solar cells and reduce losses. There are three main losses in solar cells: thermal [6], electrical [7] and optical [8]. More than 30 % of the light incident on a silicon-based solar cell is reflected [9]. To reduce this reflection coefficient, methods have been developed to cover the surface of the solar cell with various anti-reflection layers [10] and to form textures [11]. The surface of silicon-based solar cells is mainly coated with SiN_x and SiO_2 because they have passivation properties and the refractive index is between the refractive indices of air and silicon [12, 13]. Theoretical calculations show that the maximum absorption coefficient is achieved when the surface of a silicon-based solar cell is coated with pyramidal textures with a base angle of 73.12° [14], but pyramidal textures with a base angle of 57.4° [15] in industry. Because in practice, alkalis or acids are used to create textures, and silicon with a crystal orientation of (100) in the solar cell is used [16]. Since the band gap of silicon is 1.12 eV, it mainly absorbs light in the visible spectrum. According to the efficiency function of solar cells, the material does not absorb photons with a lower energy than the band gap energy. If the energy of the photons is much greater than the band gap energy, then they produce hot electrons. High-energy hot electrons quickly dissipate their energy to form a phonon and become valence electrons again. Therefore, it cannot participate in the formation of current. Therefore, luminescent materials [17] or metal nanoparticles [18] are used to modify the absorption spectrum of solar cells.

Silicon-based solar cells are the most sensitive devices to the environment. The effects of light intensity [19], temperature [20] and the angle of incidence [21] on the solar cell have been studied. As the temperature increases, the short-circuit current increases slightly and the open circuit voltage decreases significantly, so the efficiency in general decreases. Therefore, various systems are being developed to cool solar panels. The surface temperature of solar panels is much higher than the ambient temperature, so the output power is reduced by almost 30 %. To prevent this, cooling through water or a ventilation system is suggested. In these cases, water is wasted, and the ventilation system requires a lot of energy. Therefore, the development of resource and energy-efficient cooling systems has become one of the main tasks in science.

Making photovoltaic devices in 3D and rotating them around their own axis can help for cooling. Photoelectric devices in 3D format can be made in the form of a prism or a pyramid. The surface of these devices is covered with solar cells, mainly solar cells cut into two types: triangles and rectangles. Because it is sufficient to use rectangular solar cells to cover the surface of a simple prism-shaped photoelectric device with full solar cells, but it is advisable to use triangular solar cells to completely cover the surface of a pyramid-shaped device. Of

* jasurbekgulomov@yahoo.com

course, when the shape of solar cells changes, their photoelectric parameters also change slightly depending on the type of material. It is therefore important to study mono- and polycrystalline silicon-based solar cells in various shapes.

2. MATERIALS AND METHODS

Theoretical, modeling and experimental methods are mainly used in the study of solar cells. In this research, experiments on the Sinton Suns-V_{oc} device and modeling techniques in the Sentaurus TCAD program were used.

2.1 Experiment

A 20 mm diameter diamond disk rotating at a speed of 35,000 rpm was used to cut silicon-based solar cells with various shapes and sizes. In industry, lasers are mainly used to cut solar cells. Therefore, in this scientific work, lasers were also tested to cut solar cells. However, when the laser was used, a shunt was formed at the edges of the solar cell, which negatively affected the quality of the solar cell. Therefore, a mechanical method was used to cut solar cells. Samples were made by cutting traditional monocrystalline and polycrystalline silicon-based solar cells into triangles and rectangles. Samples of solar cells with an area of 5.2×5.2 cm^2 were cut in the middle of the side to form a rectangle and diagonally to form triangular surfaces.

Xenon lamp with solar light intensity, high-precision voltmeter, ammeter and resistors sets was used to measure *I-V* characteristics of solar cells. A Sinton Suns-V_{oc} device was used to measure the dependence of the open circuit voltage on the light intensity.

A hexagonal prism-shaped photovoltaic device, which can freely rotate around its own axis, is made of polycrystalline silicon-based solar cells with an area of 5.2×5.2 cm^2. Four elements were placed on each surface of the prism, and they were connected in series. Blocks consisting of cells on each surface of the prism were also connected in series. Therefore, this prism-based photovoltaic device is created by connecting 24 elements in series.

A parabolic reflector was placed on the back of the prism-based photovoltaic device to illuminate it from all sides. The characteristics of the device were measured in two different states: rotating and non-rotating. The characteristics of the device in the non-rotating and rotating states were measured under the same environmental conditions using a high-precision voltmeter, ammeter, thermometer, tachometer and resistance sets. A DC motor was used to rotate the device and a potentiometer was used to change its rotational speed. Because the rotational speed of the motor can be controlled by changing the voltage. The surface temperature of the device was measured using a thermometer and the rotational speed was determined using a tachometer.

2.2 Simulation

Many programs have been developed to model solar cells. The most widely used of these are Lumerical TCAD, Sentaurus TCAD, and Silvaco TCAD. Sentaurus TCAD was used in this research.

A geometric model of solar cells was created in the Sentaurus Structure Editor. The algorithmic method of creating geometric model is described in detail in our previous scientific works. To study the effect of the shape of the solar cell on its performance, 3D geometric models were developed. Solar cells are basically made up two types of triangles and rectangles because the experimental samples were also triangular and rectangular. Phosphorus atoms with a concentration of $1{\cdot}10^{17}$ cm^{-3} were introduced in the *n*-region and boron atoms with a concentration of $1{\cdot}10^{15}$ cm^{-3} in the *p*-region. The thickness of the *n*-region was taken to be 1 μm and the thickness of the *p*-region was 9 μm. A rectangular surface solar cell consists of an equilateral right-angled triangle with sides of 10×5 μm^2 and a triangular surface with a surface area of 10 μm. The samples were made in the same way as in the experiment, geometric models of solar cells with a surface area of 10×10 μm^2, cut in half in the middle of the side of the solar cell to form rectangular solar cell and cut in half through diagonal to form triangular solar cell.

In this paper, geometric models were developed because of the use of numerical methods in modeling solar cells. The minimum size of the meshes was 0.2 μm and the maximum size was 0.2 μm. After creating geometrical models in the Sentaurus device, material properties were given, and calculations were performed.

2.3 Theoretical Background of Simulation

Modeling of semiconductor devices is the determination of the principle of operation of a device and its parameters using experimentally determined material properties and fundamental theories. Depending on the structure of the semiconductor device, modeling can range from simple to complex. The simplest semiconductor device is a diode. The basis of a solar cell is also a diode. However, solar cells are part of semiconductor devices that are difficult to model because they are optoelectronic devices, and modeling is done in two stages. At the first stage, optical properties are determined. Three different methods, Ray Tracing, Transfer Matrix Method (TMM) and Beam Propagation are widely used. In this scientific study, the TMM method was used to determine optical properties. TMM calculates relationship between the energies of incident, reflected, and transmitted rays using a matrix as given below by formula (1):

$$\begin{bmatrix} E_i \\ E_r \end{bmatrix} = M \begin{bmatrix} E_t \\ 0 \end{bmatrix}. \quad (1)$$

Here, M is the matrix, E_i is the electric field of incident light E_r is the electric field of reflected light, and E_t is the electric field of transmitted light.

Since solar cells have different media such as air/silicon intersections, optical boundary conditions must be given. Optical boundary conditions are divided into two depending on the parameters of light: energy and angle. The relationship between the energies of incident, reflected, and transmitted rays at the boundary between two media is determined using the Fresnel formulas given in Eq. (2):

$$\begin{cases} r_t = \dfrac{n_1 \cos\beta - n_2 \cos\gamma}{n_1 \cos\beta + n_2 \cos\gamma}, \\ t_t = \dfrac{2n_1 \cos\beta}{n_1 \cos\beta + n_2 \cos\gamma}, \end{cases} \quad \begin{cases} r_p = \dfrac{n_1 \cos\gamma - n_2 \cos\beta}{n_1 \cos\gamma + n_2 \cos\beta}, \\ t_p = \dfrac{2n_1 \cos\beta}{n_2 \cos\beta + n_1 \cos\gamma}. \end{cases} \tag{2}$$

Here, r_t and t_t are the Fresnel coefficients for transversal polarized light, r_p and t_p are the Fresnel coefficients for parallel polarized light, n_1 and n_2 are the refractive indices of the first and second media, β is the angle of incident light as well as γ is the angle of refracted light.

The relationship between the angles at the boundary of the two media is determined by Snelli's law given in formula (3):

$$\frac{n_1}{n_2} = \frac{\sin(\gamma)}{\sin(\theta)}, \quad \beta = \theta, \tag{3}$$

where θ is the angle of reflected light.

Using TMM and optical boundary conditions, the basic optical parameters of a solar cell are determined. To continue modeling logically, a quantum yield function and optical generation are calculated using Burger-Lambert's law. Quantum yield function is a logical function, in which the photon energy absorbed by a solar cell is equal to 1 if the material used in a solar cell is greater than the band gap, so it forms an electron-hole pair, and 0 if it is small. This means that the photon is not absorbed, and no electron-hole pair is formed. Using this method, the concentration of photogenerated charge carriers in volume of the solar cell is determined.

After calculating the optical properties, the electrical properties are determined. The most important for this is the Poisson equation given in formula (4):

$$\Delta\varphi = -\frac{q}{\varepsilon}(p - n - N_D + N_A). \tag{4}$$

Here, ε is the permittivity, n and p are the concentrations of electrons and holes, N_D and N_A are the concentrations of donors and acceptors, q is the electron charge.

The concentrations p and n of charge carriers in the Poisson equation are determined using the Fermi function given in formula (5):

$$\begin{aligned} n &= N_c F_{1/2}\left(\frac{E_{F,n} - E_c}{kT}\right), \\ p &= N_V F_{1/2}\left(\frac{E_V - E_{F,p}}{kT}\right). \end{aligned} \tag{5}$$

Here, N_c and N_v are the densities of states in the conduction and valence bands, E_c is the minimum energy of the conduction band, E_v is the maximum energy of the valence band, T is the temperature, k is the Boltzmann constant, $E_{F,n}$ and $E_{F,p}$ are the quasi Fermi energies.

The p-n junction in a solar cell creates an internal electric field and separates electron-hole pairs. Then the charge carriers will transfer. The transport of charge carriers generates electricity. There are basically four models in the Sentaurus TCAD to calculate charge transport: Drift-Diffusion, Thermodynamics, Hydrodynamics, and Monte Carlo. Since the effect of temperature on the solar cell was not taken into account in this scientific work, the Drift-Diffusion model given in formula (6) was used to calculate the charge transport:

$$\begin{aligned} \vec{J}_n &= \mu_n(n\nabla E_C - 1.5nkT\nabla\ln m_n) + D_n(\nabla n - n\nabla\ln\gamma_n), \\ \vec{J}_p &= \mu_p(p\nabla E_V + 1.5pkT\nabla\ln m_p) - D_p(\nabla p - p\nabla\ln\gamma_p). \end{aligned} \tag{6}$$

Here, J_n and J_p the are electron and hole currents, m_n and m_p are the effective masses of electrons and holes, γ_n and γ_p are the coefficients of Fermi function, D_n and D_p are the diffusion coefficients of electrons and holes, μ_n and μ_p are the mobilities of electrons and holes.

The Masetti formula [22] was used to calculate the mobility of charge carriers. The Masetti empirical formula takes into account the effect of temperature, doping concentration, and phonon scattering on the mobility of charge carriers. Since silicon is an indirect semiconductor, radiative recombination is not considered in the modeling of silicon-based devices. Therefore, only Auger and Shockley-Read-Hall (SRH) recombinations are considered.

Metal contacts play an important role in the quality of solar cells. In this scientific study, an ohmic contact was made at the top and bottom of the solar cell. Since the calculation is performed in numerical methods, the electrical boundary conditions must also be included in the model. Due to the formation of an ohmic transition between the contact and the semiconductor, the ohmic boundary conditions given in formula (7) were used:

$$\begin{aligned} &\vec{J}_m \cdot \hat{n} = (\vec{J}_n + \vec{J}_p + \vec{J}_D)\cdot\hat{n}, \\ &\varphi = \Phi_M - \Phi_0, \\ &n = n_0, \\ &p = p_0. \end{aligned} \tag{7}$$

Here, J_m is the current in metals, J_D is the diffusion current, φ is the electrostatic potential, Φ_M is the Fermi potential of a metal, Φ_0 is the electrostatic potential in equilibrium, n_0 and p_0 are the doping concentrations of electrons and holes in equilibrium.

3. RESULTS AND DISCUSSION

3.1 Experimental Measurements of Characteristics of Solar Cells with Various Shapes

The Suns-*Voc* characteristic is mainly used to determine the quality of solar cells. Using this characteristic, it is possible to assess the passivation and contact quality of the front and rear surfaces of the solar cell. In the experiment, Sinton devices were used to determine the Suns-V_{oc} characteristics of solar cells. Fig. 1 also illustrates the dependence of the open circuit voltage of polycrystalline (a) and monocrystalline (b) silicon-based rectangular and triangular solar cells with an experimental size of 1352 mm^2 on the light intensity. The open circuit voltage of the rectangular polycrystalline silicon-based solar cells was relatively high in the triangular

shape at low light intensities. For example, at a light intensity of 0.1 suns, the open circuit voltage of a rectangular solar cell was found to be 0.06 V relative to that of a triangular solar cell. When the intensity of the light increased, the difference became smaller. The difference in light intensity is reduced to 0.01 V. This is because the generation rate is lower at low light intensities. Recombination plays a key role in determining the quality of solar cells. Due to the presence of granular boundaries in polycrystalline silicon, the recombination rate is higher. In addition, the perimeter of a rectangle of the same surface is smaller than that of a triangle. The transport of charge carriers on the edges of the solar cell increases their recombination due to dangling bonds on the surface and edges of the solar cell, the defects are larger than the size [23]. Incomplete bonds, on the other hand, hold oxygen and form recombination centers. The front and back surfaces of solar cells are passivated using SiN_x or SiO_2, but their sides are not passivated. When the intensity of light incident on a polycrystalline silicon-based solar cell increases, generation rate increases. Therefore, the effect of shape on the performance of polycrystalline silicon is also reduced. Thus, in a polycrystalline silicon-based solar cell, it was found that the shape change mainly affects the recombination rate. In a monocrystalline silicon-based solar cell, the open circuit voltage of a triangular solar cell is higher than that of a rectangular one. In addition, the difference between the open circuit voltages also increases as the intensity increases. Since recombination in monocrystalline silicon occurs only due to the ionization of doping atoms and their conversion into recombination centers [24], the voltage difference is very small even at low intensities. As the intensity increases, photogeneration rate increases. A sharp increase in the amount of charge carriers increases the probability of electron scattering in monocrystalline silicon-based solar cells [25].

The pseudo *I-V* characteristic of solar cells can also be measured in the Sinton Suns-V_{oc} device. Fig. 2 shows the pseudo *I-V* characteristics of polycrystalline (a) and monocrystalline (b) silicon-based rectangular and triangular solar cells with an area of 1352 mm². For a polycrystalline silicon-based solar cell, the rectangular shape achieves better *I-V* characteristics. In monocrystalline silicon, the triangular shape has better *I-V* characteristics. However, the difference in *I-V* characteristics in the monocrystalline silicon-based solar cell is very small.

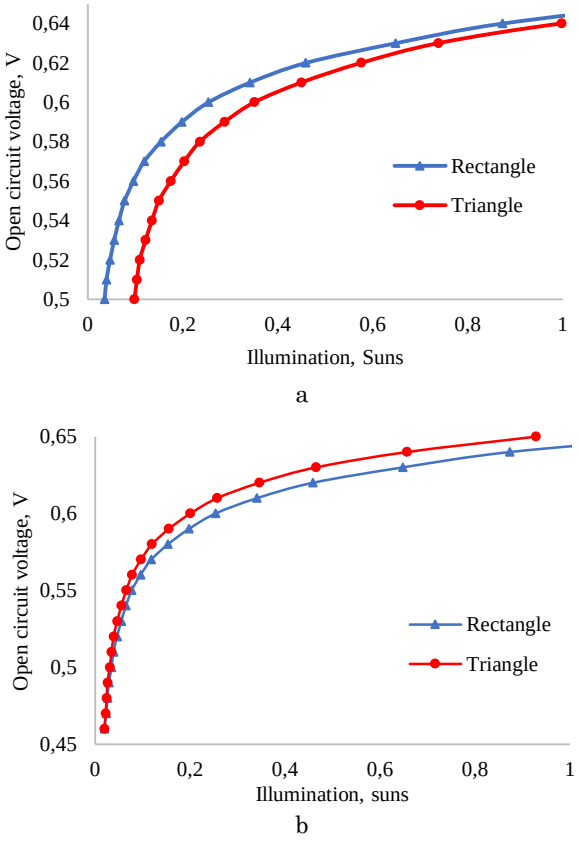

Fig. 1 – Dependence of the open circuit voltage of polycrystalline (a) and monocrystalline (b) silicon-based rectangular and triangular solar cells with an area of 1352 mm² on the light intensity

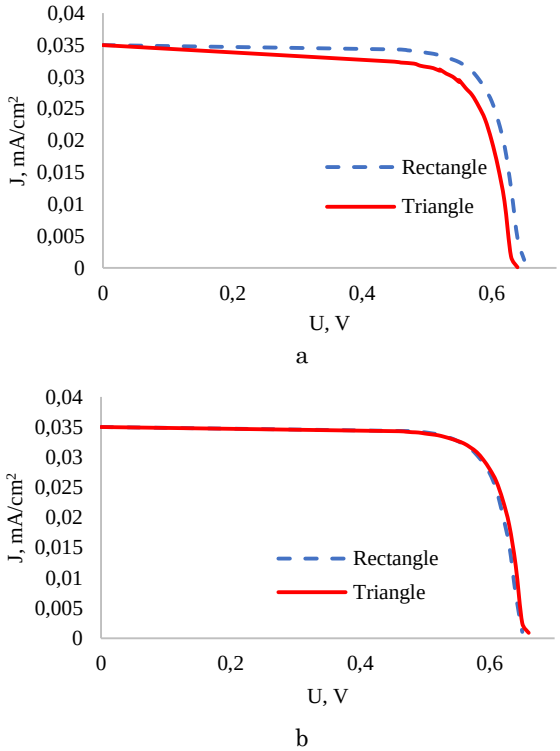

Fig. 2 – *I-V* characteristics of polycrystalline (a) and monocrystalline (b) silicon-based rectangular and triangular solar cells with an area of 1352 mm²

3.2 Simulation of Solar Cells with Various Shapes

Monocrystalline silicon-based solar cells of various shapes were modeled in 3D. When shape of a solar cell changes, its charge carriers and current distribution also change. Therefore, Fig. 3 shows the current density distribution in a silicon-based solar cell in the form of a parallelepiped (a) and a triangular prism (b) with equal active surfaces. The current distribution on the opposite side of the contact of the solar cell in the form of a parallelepiped is determined as the minimum. This means that charge carriers in this area can reach the contacts. In a triangular prism-shaped solar cell, the distribution of current density at the opposite contact angle is minimal, while at the other angles it is average.

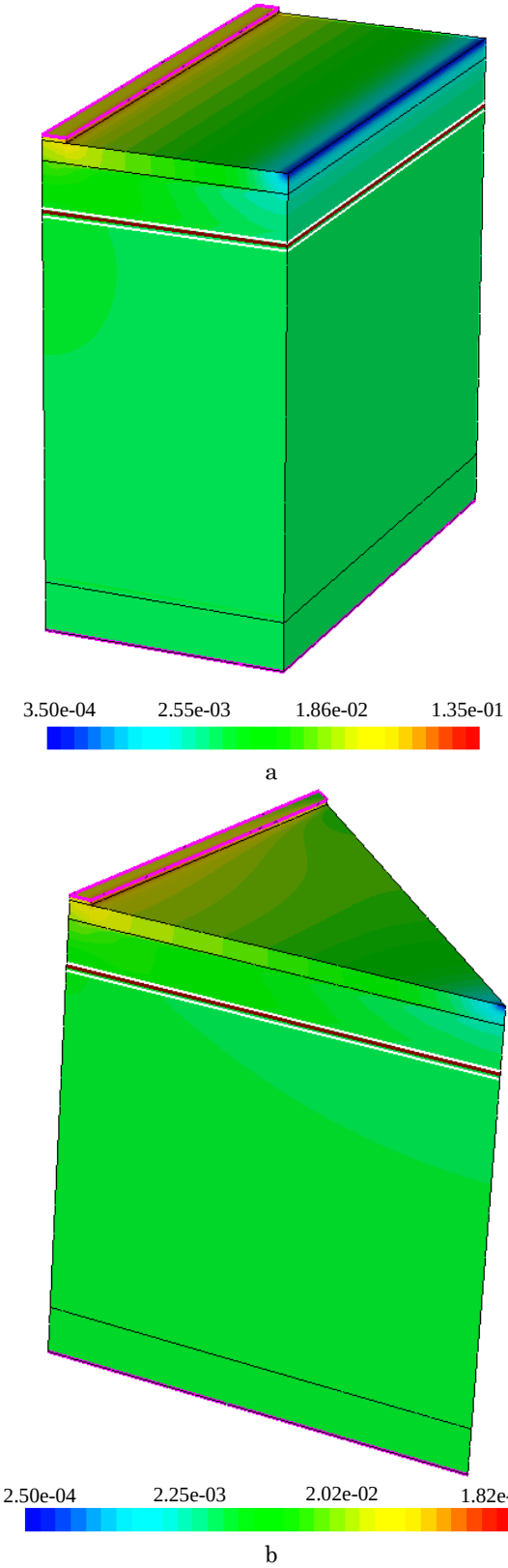

Fig. 3 – Current density distribution in a silicon-based solar cell in the form of a parallelepiped (a) and a triangular prism (b) with equal active surfaces [unit: mA/cm^2]

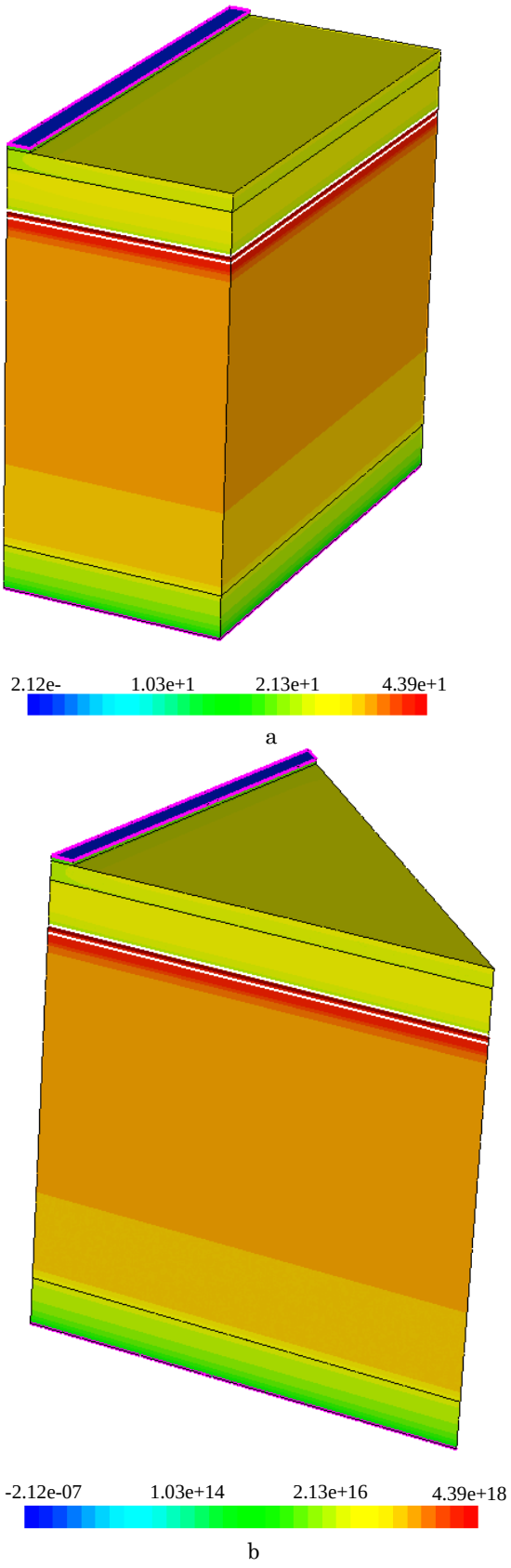

Fig. 4 – SRH recombination distribution in a silicon-based solar cell in the form of a parallelepiped (a) and a triangular prism (b) with equal active surfaces [unit: $sm^{-3}s^{-1}$]

Fig. 4 shows the distribution of the SRH recombination rate in a silicon-based solar cell in the form of a parallelepiped (a) and a triangular prism (b) with equal active surfaces. For both cells, the recombination distribution is found to be almost identical across the layers. The distribution describes the recombination rate in the base area because the SRH recombination in the base area is greater than that of the Auger recombination. When the input concentration exceeds the critical value, the SRH recombination does not increase, but the rate of Auger recombination increases sharply. Therefore, the rate of Auger recombination in the emitter region and SRH recombination in the base region will be large.

I-V characteristics are mainly used to compare solar cells with each other. Therefore, in this paper, the *I-V* characteristics of a silicon-based solar cell in the form of a parallelepiped (a) and a triangular prism (b) with equal active surfaces are determined by modeling and shown in Fig. 5. The *I-V* characteristics are almost the same, but the short-circuit current of a triangular prism-shaped solar cell is found to be greater ($1.657 \cdot 10^{-12}$ A). Hence, the result obtained in the modeling is suitable to the experimental results. In other words, in monocrystalline silicon-based solar cells, a triangular prism-shaped solar cell is better than a parallelepiped in experiments and modeling.

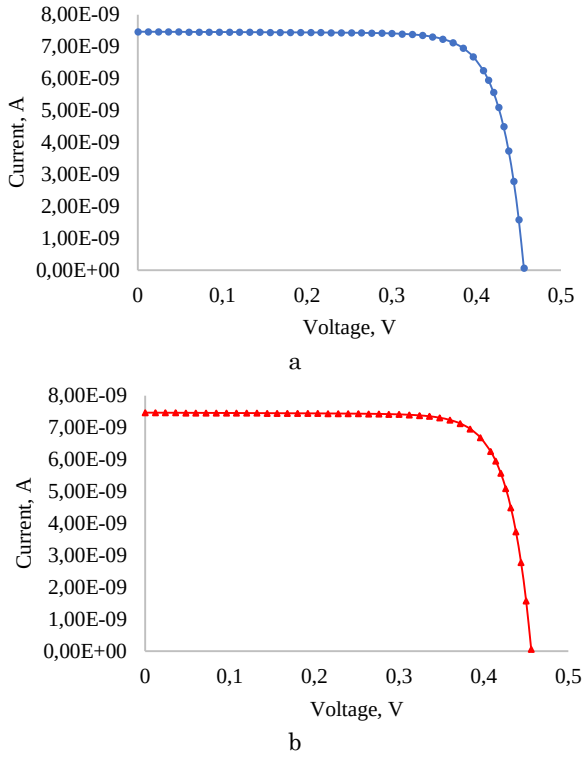

Fig. 5 – Volt-ampere characteristics of a silicon-based solar cell in the form of a parallelepiped (a) and a triangular prism (b) with equal active surfaces

3.3 Photovoltaic Device in 3D Format

The above results show that the photoelectric parameters of the rectangular polycrystalline silicon-based solar cell are good. Therefore, a hexagonal prism-shaped photoelectric device was made from a rectangular polycrystalline silicon-based solar cell. Fig. 6 shows the *I-V* characteristics of a stationary and rotating cases of a prism-shaped 3D photovoltaic device formed by a series connection of 24 silicon-based solar cells with an area of 56×56 mm^2. When the device is rotating, the short-circuit current is 151 mA and the open circuit voltage is 12980 mV, and when it is not rotating, the short-circuit current is 149.6 mA and the open circuit voltage is 12820 mV. The purpose of rotating the device is to create a wind effect around it. Yavuzdeger also rotated a 3D photovoltaic device around its axis for cooling and used a neural network to determine its optimal parameters and compare them with conventional solar panels [26].

It was found that the photoelectric parameters of the device improved when it rotated. Therefore, the dependence of its photoelectric parameters on the rotational speed was studied. Fig. 7 illustrates the dependence of the open circuit voltage (a) and surface temperature (b) of a 3D photovoltaic device on the angular velocity of the device. When the angular velocity increases, the open circuit voltage increases, and the surface temperature of the device decreases. When the temperature of the solar cell decreases, its open circuit voltage increases. This is due to the increase in the band gap energy and the decrease in the concentration of intrinsic carriers. The cooling of ordinary solar panels by wind has been widely studied. Also, in solar panels made of polycrystalline silicon, the dependence of the amount of heat released per unit time on the surface of the solar panel is well studied in Skoplaki's work [27]. When the device rotates, airflow occurs around it. The velocity of air molecules around the device can be assumed to be equal to the linear velocity of the device endpoints. Therefore, when the speed of rotation of the device changes, the temperature of its surface also changes.

The surface temperature of the device was 50 °C without rotation and the open circuit voltage was 13.12 V. In the range of 0-6 rad/s of rotation speed, the open circuit voltage of the device increased sharply by 0.36 V and the surface temperature decreased by 9.4 °C. In the range of 6-8 rad/s, the open circuit voltage increased slightly by 0.01 V, and the temperature decreased by 1.1 °C accordingly. This means that when the

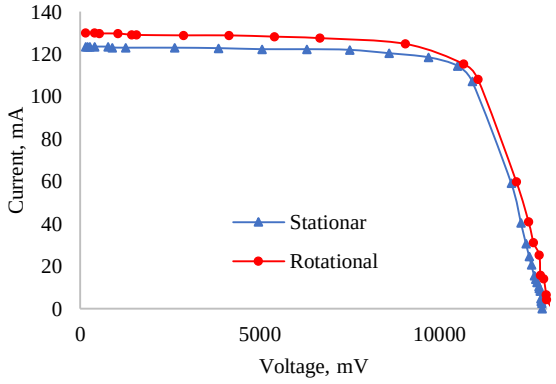

Fig. 6 – *I-V* characteristics in stationary and rotating cases of a prism-shaped 3D photovoltaic device consisting of a series connection of 24 silicon-based solar cells with an area of 56×56 mm^2

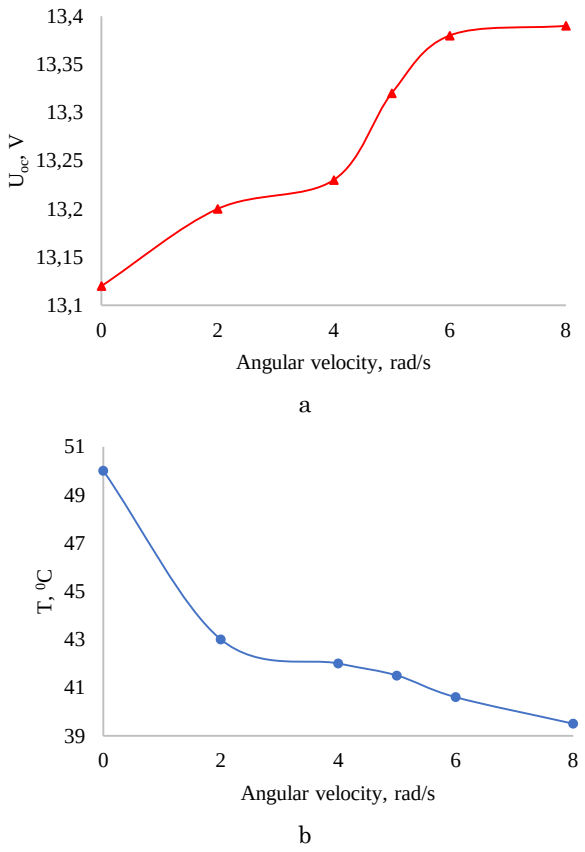

Fig. 7 – Dependence of the open circuit voltage (a) and surface temperature (b) on the angular velocity of the device

speed of a photovoltaic device increases, its open circuit voltage increases asymptotically to a certain value, and the surface temperature decreases asymptotically close to the ambient temperature but cannot be lower than the ambient temperature. Therefore, the use of this method can prevent the surface of the photovoltaic device from overheating but cannot cool it to low temperatures.

4. CONCLUSIONS

Experimental studies of mono- and polycrystalline silicon-based solar cells of triangular and rectangular shapes have shown that the photoelectric parameters are better when the monocrystalline silicon-based solar cell is cut in a triangular shape and the polycrystalline silicon-based solar cell is cut in a rectangular shape. Therefore, it was proposed to use rectangular monocrystalline silicon-based solar cells in the construction of prism-shaped photoelectric devices and triangular-shaped monocrystalline silicon-based solar cells in the construction of pyramid-shaped photoelectric devices. Even when triangular and rectangular monocrystalline silicon-based solar cells were modeled in Sentaurus TCAD, it was found that the photoelectric parameters of the triangular solar cell were better, and the efficiency was higher. The results obtained in the modeling were consistent with the experimental results. Based on the above results, a prism-shaped photoelectric device was made from a rectangular solar cell based on polycrystalline silicon, and its characteristics were determined experimentally. It was found that as the rotational speed of the device increased, the surface temperature of the photoelectric device decreased, and the open circuit voltage increased asymptotically to a certain value. The surface temperature of the photovoltaic device cannot be lower than the ambient temperature. Therefore, to effectively use the device, it is possible to change the rotation speed of the photovoltaic device depending on the ambient temperature.

ACKNOWLEDGEMENTS

This work is supported by Fundamental Research Project of Uzbekistan (FZ-2020092973).

REFERENCES

1. P.A. Østergaard, N. Duic, Y. Noorollahi, H. Mikulcic, S. Kalogirou, *Renew. Energy* **146**, 2430 (2020).
2. A. Mardani, A. Jusoh, E.K. Zavadskas, F. Cavallaro, Z. Khalifah, *Sustainability* **7** No 10, 13947 (2015).
3. P. Fath, S. Keller, P. Winter, W. Jooß, W. Herbst, *Conference Record of the IEEE Photovoltaic Specialists Conference* (2009).
4. A. Blakers, N. Zin, K.R. McIntosh, K. Fong, *Energy Procedia* **33**, 1 (2013).
5. W. Shockley, H.J. Queisser, *J. Appl. Phys.* **32** No 3, 510 (1961).
6. L. Xu, et al., *Joule* **5**, No 3, 631 (2021).
7. Y.Q. Gu, C.R. Xue, M.L. Zheng, *Adv. Mat. Res.* **953**, 91 (2014).
8. B. Hoex, M. Dielen, M. Lei, T. Zhang, C.Y. Lee, *AIP Conf. Proc.* **1999**, No 1, 040010 (2018).
9. I.P. Buryk, L.V. Odnodvorets, Ya.V. Khyzhnya, *J. Nano-Electron. Phys.* 13 No 1, 01012 (2021).
10. S. Jun Jang, et al., *Opt. Exp.* **19**, No 102, A108 (2011).
11. S.C. Baker-Finch, K.R. McIntosh, *Prog. Photovolt.: Res. Appl* **21** No 5, 960 (2013).
12. Y. Wan, K.R. McIntosh, A.F. Thomson, *AIP Adv.* **3** No 3, 032113 (2013).
13. S.W. Glunz, F. Feldmann, *Sol. Energy Mater. Sol. C.* **185**, 260 (2018).
14. J. Gulomov, R. Aliev, *Sci. Tech. J. Inf. Technol. Mech. Opt.* **21** No 5, 626 (2021).
15. K. Kim, S.K. Dhungel, S. Jung, D. Mangalaraj, J. Yi, *Sol. Energy Mater. Sol. C.* **92** No 8, 960 (2008).
16. H. Park, S. Kwon, J.S. Lee, H.J. Lim, S. Yoon, D. Kim, *Sol. Energy Mater. Sol. C.* **93** No 10, 1773 (2009).
17. X. Huang, S. Han, W. Huang, X. Liu, *Chem. Soc. Rev.* **42** No 1, 173 (2012).
18. J. Gulomov, R. Aliev, *Phys. Chem. Solid State* **22** No 4, 756 (2021).
19. J. Gulomov, R. Aliev, *Nanosystems: Phys. Chem. Math.* **12** No 5, 569 (2021).
20. J. Gulomov, R. Aliev, *J. Nano- Electron. Phys.* **13** No 4, 04033 (2021).
21. J. Gulomov, R. Aliev, *J. Nano- Electron. Phys.* **13** No 6, 06036 (2021).
22. M. Sotoodeh, A.H. Khalid, A.A. Rezazadeh, *J. Appl. Phys.* **87** No 6, 2890 (2000).
23. T.P. Weiss, B. Bissig, T. Feurer, R. Carron, S. Buecheler, A.N. Tiwari, *Sci. Rep.* **9** No 1, 1 (2019).
24. R. Gogolin, N.P. Harder, *J. Appl. Phys.* **114** No 6, 064504 (2013).
25. J. Xi, D. Wang, Y. Yi, Z. Shuai, *J. Chem. Phys* **141** No 3, 034704 (2014).
26. A. Yavuzdeger, F. Ekinci, *IETE J. Res.* (2021).
27. E. Skoplaki, J.A. Palyvos, *Renew. Energy* **34** No 1, 23 (2009).

Дослідження моно- та полікристалічних кремнієвих сонячних елементів різної форми для фотоелектричних пристроїв у форматі 3D: експеримент та моделювання

J. Gulomov, R. Aliev, N. Mirzaalimov, B. Rashidov, J. Alieva

Andijan State University, 129, Universitet St., 170100 Andijan, Uzbekistan

При підвищенні температури ефективність сонячних елементів падає, тому проектування та побудова фотоелектричних пристроїв із системою охолодження із сонячних елементів замість сонячних панелей є одним із найважливіших завдань сьогодення. В даній науковій роботі були досліджені різні форми фотоелектричних пристроїв у форматі 3D, які можуть охолоджуватися шляхом обертання навколо власної осі. У цих пристроях використовуються переважно трикутні та прямокутні сонячні елементи, тому вплив форми поперечного перерізу на фотоелектричні параметри монокристалічних та полікристалічних кремнієвих сонячних елементів досліджено експериментально та за допомогою моделювання. Результати показали, що сонячні елементи на основі полікристалічного кремнію можна вирізати прямокутними та використовувати у виробництві фотоелектричних пристроїв у формі призми, а сонячні елементи на основі монокристалічного кремнію можна використовувати для трикутного вирізання та у виробництві фотоелектричних пристроїв пірамідальної форми. На основі цих результатів експериментально досліджено фотоелектричний пристрій у формі шестикутної призми із прямокутного сонячного елементу на основі полікристалічного кремнію. Температура поверхні пристрою становила 50 °C без обертання, а напруга холостого ходу складала 13,12 В. У діапазоні швидкості обертання 0-6 рад/с напруга холостого ходу пристрою різко зросла на 0,36 В, а температура поверхні знизилася на 9,4 °C.

Ключові слова: Монокристал, Полікристал, Кремній, Сонячний елемент, Фотоелектричний пристрій, Моделювання, Форма.